Journal of
Synchrotron
Radiation

ISSN 1600-5775

Received 12 March 2014
Accepted 7 May 2014

Data analysis method to achieve sub-10 pm spatial resolution using extended X-ray absorption fine-structure spectroscopy

Yonghua Du,[a]*‡ Jia-ou Wang,[b]‡ Longhua Jiang,[c] Lucas Santiago Borgna,[a] Yanfei Wang,[d]* Yi Zheng[e] and Tiandou Hu[b]

[a]Institute of Chemical and Engineering Sciences, A*STAR, Singapore 627833, Singapore, [b]Institute of High Energy Physics, Chinese Academy of Sciences, Beijing 100049, People's Republic of China, [c]Department of Physics, Pennsylvania State University, University Park, PA 16802, USA, [d]Institute of Geology and Geophysics, Chinese Academy of Sciences, Beijing 100029, People's Republic of China, and [e]Department of Chemistry, National University of Singapore, Singapore 117543, Singapore. *E-mail: yonghua.du@gmail.com, yfwang@mail.iggcas.ac.cn

Obtaining sub-10 pm spatial resolution by extended X-ray absorption fine structure (EXAFS) spectroscopy is required in many important fields of research, such as lattice distortion studies in colossal magnetic resistance materials, high-temperature superconductivity materials *etc.* However, based on the existing EXAFS data analysis methods, EXAFS has a spatial resolution limit of $\pi/2\Delta k$ which is larger than 0.1 Å. In this paper a new data analysis method which can easily achieve sub-10 pm resolution is introduced. Theoretically, the resolution limit of the method is three times better than that normally available. The method is examined by numerical simulation and experimental data. As a demonstration, the $LaFe_{1-x}Cr_xO_3$ system (x = 0, 1/3, 2/3) is studied and the structural information of FeO_6 octahedral distortion as a function of Cr doping is resolved directly from EXAFS, where a resolution better than 0.074 Å is achieved.

© 2014 International Union of Crystallography

Keywords: EXAFS; spatial resolution; atom distribution function.

1. Introduction

EXAFS (Sayers *et al.*, 1971) is a powerful technique for probing the local structure around absorbing atoms, which has been widely applied to material science, chemical engineering, environmental science and engineering, life science *etc.* However, there is still an unsolved limitation of EXAFS: insufficient spatial resolution. Based on the existing EXAFS data analysis methods, EXAFS has a resolution limit of $\Delta r \geq \pi/2\Delta k$ (Lee *et al.*, 1981; Teo, 1986), where Δr is the spatial resolution and Δk is the wavenumber in the EXAFS data. For the typical case of oxygen as the nearest neighbours, Δk is usually less than 15 $Å^{-1}$, so the best spatial resolution is larger than 0.1 Å. Exceeding this limit may lead to unreliable results. Stern (2001) also emphasized that 'any claim of a higher resolution (higher than 0.1 Å) of Δr for two O atoms should be suspect'.

However, sub-10 pm spatial resolution is required in many important fields of research, such as lattice distortion studies in colossal magnetic resistance (CMR) materials (Sen *et al.*, 2010), high-temperature superconductivity materials (Saha *et al.*, 2009), antiferromagnetic materials (de la Cruz *et al.*, 2010) and multiferroic materials (Gupta *et al.*, 2013). It is believed that the lattice distortion plays an important role in the special properties of these materials and a detailed structural analysis can help to better understand the physics of these materials. Scientists have applied EXAFS to these materials. However, due to the insufficient resolution, they have to guess the number of atom shells for curve fitting (Haas *et al.*, 2004; Pandey *et al.*, 2006) which may lead to 'suspect' results (Stern, 2001). Alternatively, they have to assume only one shell exists and focus on the Debye–Waller factor (DWF) (Booth *et al.*, 1998; Sundaram *et al.*, 2009; Chu *et al.*, 2013), losing important structural information.

Indeed, EXAFS is the ideal method to study lattice distortion because it is an element-sensitive method for crystalline and non-crystalline samples. Furthermore, it has an accuracy of 0.01–0.001 Å (Dalba *et al.*, 1999) for interatomic distance determination. The key issue is how to improve the spatial resolution. Several attempts to improve the resolution have been carried out using the regularization method (Tikhonov & Arsenin, 1981; Babanov *et al.*, 1981; Yang & Bunker, 1996; Rossberg & Funke, 2010) and the wavelet method (Funke *et al.*, 2007; Penfold *et al.*, 2013). However, the improved resolution does not surpass the 0.1 Å limit. In one of the latest works, Rossberg & Funke (2010) attempted to resolve two peaks with Δr = 0.15 Å using the regularization

‡ These authors contributed equally to this work.

method; however, they were unable to resolve these peaks directly. Although the regularization method has a higher spatial resolution than the Fourier transform (FT) method because it can reduce the peak broadening in r space caused by limited data in k-space, it cannot provide a spatial resolution better than 0.1 Å. The neutron/X-ray pair distribution function (PDF) method (Toby & Egami, 1992) is a powerful method for obtaining the PDF of samples with high spatial resolution, with the resolution limit of the PDF method being $\Delta r \geq 2\pi/Q_{\max}$ (Fábián *et al.*, 2007), where $Q = 4\pi\sin(\theta)/\lambda$. In most cases, $Q_{\max}$ is smaller than 60 Å^{-1} so it is difficult to obtain sub-10 pm resolution using the PDF method.

The regularization method cannot provide a sub-10 pm resolution due to the DWF. In the existing EXAFS data analysis models, the DWF is coupled with the structural information, broadening the peak of each atom shell in r-space significantly and, therefore, affecting the spatial resolution. In this paper, we raise a model which separates the DWF from the structure information, and propose an algorithm based on the gradient descent algorithm to solve this model. This algorithm is a non-parametrical algorithm which allows us to obtain structural information directly from EXAFS data without assuming the number of fitting parameters. Our method is tested by numerical simulation and experimental data of the $LaFe_{1-x}Cr_xO_3$ system (x = 0, 1/3, 2/3). As a result, sub-10 pm spatial resolution is achieved.

2. Modelling and algorithm description

The general EXAFS integral equation has the following form,

$$\chi(k) = \int_0^\infty A(k, r)g(r)\,\mathrm{d}r, \tag{1}$$

where $g(r)$ is a function which contains all structural information of the EXAFS spectrum, including coordination numbers, bond lengths and DWF. The kernel function A is in the form

$$A(k, r) = \frac{S_0^2(k)F(k, r)}{kr^2}\exp[-2r/\lambda(k)]\sin[2kr + \varphi(k, r)],$$

in which $F(k, r)$ is the effective backscattering amplitude, S_0^2 is the amplitude reduction factor, $\lambda(k)$ is the mean free path of the photoelectron, k is the photoelectron wavevector, r is the interatomic distance, $\varphi(k, r)$ is the phase shift due to the atomic potentials and $\chi(k)$ is the EXAFS function.

For the regularization method, $g(r)$ is the target to be solved. As mentioned previously, $g(r)$ contains all the structural information and the DWF. Therefore, the spatial resolution will be significantly decreased. Hence, we will separate the DWF from $g(r)$, which will theoretically lead to a significantly higher spatial resolution than the regularization method.

Assuming that $g(r)$ satisfies a Gaussian model (Rossberg & Funke, 2010),

$$g(r) = \sum_{j=1}^{\text{shells}} \frac{n_j}{\left(2\pi\sigma_j^2\right)^{1/2}}\exp\left[-(r - r_j)^2/2\sigma_j^2\right]. \tag{2}$$

Thus, the integral in (1) can be resolved analytically and, using justified approximations, is reduced to the EXAFS equation for a given number of coordination shells (Sayers *et al.*, 1971),

$$\chi(k) = \sum_{j=1}^{\text{shells}} \frac{n_j S_0^2(k)F_j(k)}{kr_j^2}\exp\left(-2\sigma_j^2k^2\right) \times \exp\left[-2r_j/\lambda(k)\right]\sin\left[2kr_j + \varphi_j(k)\right], \tag{3}$$

in which n_j is the coordination number and σ_j^2 is the DWF of the backscattering atoms in the jth shell. Converting to the integral form, (3) becomes

$$\chi(k) = \int_0^R A(k, r)\exp\left[-2\sigma(r)^2k^2\right]n(r)\,\mathrm{d}r. \tag{4}$$

This is a new integral equation based on the Gaussian model. In (4), $n(r)$ is named the atom distribution function (ADF). The ADF consists of one or more peaks. The position and area of each peak are the bond length and coordination number, respectively. Theoretically, the ADF should be a δ function; however, in our case this convergence does not occur due to the restricted amount of data. Hence, the spatial resolution limit of this method is $\Delta r \geq 1/2\Delta k$, following the uncertainty principle.

In this paper, we focus on the structural analysis of lattice distortions through the nearest shells to absorbing atoms (we name these atom shells as subshells in this contribution). The advantage is that EXAFS data of the nearest subshells often have a better signal-to-noise ratio than high coordination shells and do not have multiple scattering signals. These atoms usually have the same atom species, close bond lengths and similar surrounding conditions. Therefore, all subshells can be assumed to have the same kernel function $A(k, r)\exp(-2\sigma^2k^2)$ in (4).

The remaining task is to reconstruct $n(r)$ from the kernel function and EXAFS data χ. For convenience, we rewrite (4) in a compact form,

$$\chi(k) = (Kn)(k), \tag{5}$$

where K is the operator of the kernel function that maps the distribution function into the observation space, and n is the ADF. Note that experimental EXAFS data χ may contain noise; therefore, to solve for $n(r)$, a constrained minimization problem is proposed,

$$\min_n \frac{1}{2}\|Kn - \chi\|^2, \tag{6}$$

subject to

$$n \geq 0, \tag{7}$$

$$0.1 > \sigma^2 > 0. \tag{8}$$

To solve (6) subject to (7) and (8), the Lagrangian multiplier method or gradient descent method with projection could be applied. Here, we introduce an algorithm based on the gradient descent algorithm (Wang, 2007).

We denote $f(n) = (1/2)\|Kn - \chi\|^2$. To maintain non-negativity of n, we let $n = \exp(x)$. Therefore, $f[\exp(x)] = (1/2)\|K\exp(x) - \chi\|^2$. This setting directly leads to the explicit non-negative constraints. The gradient can be deduced using the formula

$$\frac{\mathrm{d}}{\mathrm{d}\xi} f(x + \xi z)|_{\xi=0},$$

which leads to the gradient formula

$$g(n) = n .* \left[K^T(Kn - \chi)\right],$$

where .* denotes the component-wise product of two vectors. The gradient descent algorithm is based on the following formula,

$$n_{k+1} = n_k + \tau_k d_k,$$

where $d_k = -g_k$ and τ_k is the step length such that $\tau_k = \mathrm{argmin}_{\tau>0} f[\exp(x_k) + \tau d_k]$. Solving the minimization problem τ_k yields

$$\tau_k^a = \frac{\left[d_k, K^T(Kn_k - \chi)\right]}{\left[d_k, K^T(Kd_k)\right]},$$

where $[\ldots, \ldots]$ denotes the inner product of two vectors. Note that, for the non-negativity constraints, we require $\tau \in \{\tau > 0 : n_k + \tau d_k \geq 0\}$, yielding

$$\tau_k^b = \min\left\{-\frac{n_k(i)}{d_k(i)} : d_k(i) < 0\right\}.$$

Therefore, the final step length should be $\tau^* = \min\{\tau_k^a, \tau_k^b\}$. The stopping criterion is based on the norm of the gradient and the maximum iteration number. A description of the algorithm is shown below.

2.1. Algorithm

(1) At the kth step, compute the gradient of the new objective function $f[\exp(x)] = (1/2)||K\exp(x) - \chi||^2$: $g_k = n_k .* [K^T(Kn_k - \chi)]$, where $n_k = \exp(x_k)$ and .* denotes the component-wise product of two vectors.

(2) Generate the negative gradient direction: $d_k = -g_k$.

(3) Calculate the step length $\tau_k = \mathrm{argmin}_{\tau>0} f[\exp(x_k) + \tau d_k]$ such that $\tau_k^* = \max\{\tau > 0 : n_k + \tau d_k \geq 0\}$, where argmin means the one-dimensional line search for the parameter τ.

(4) Update the iterative points $n_{k+1} = n_k + \tau_k^* d_k$ until convergence.

The final values of n and σ^2 are obtained at the global minimum of equations (6)–(8).

3. Method testing

3.1. Numerical simulation

To test the resolution and reliability of our method, a numerical simulation was performed first. The parameters of this simulation were chosen based on the $LaFeO_3$ structure (Sangaletti *et al.*, 2001) to ensure that our method can work properly for $LaFe_{1-x}Cr_xO_3$ experimental data which will be applied in a later test.

The procedure to execute the numerical simulation is as follows.

(1) Build a simulated $g(r)$ using equation (2).

(2) Calculate the simulated EXAFS data $\chi(k)$ using equation (1) and add noise to $\chi(k)$.

(3) Reconstruct the ADF using the noised data.

In the simulation, $g(r)$ was built using a sum of three Gaussian peaks with $n_1 = n_2 = n_3 = 2$, $r_1 = 1.923$ Å, $r_2 = 2.013$ Å, $r_3 = 2.086$ Å. So, the minimum bond length difference is 0.074 Å. The DWF was fixed at 0.005. The backscattering amplitude $F(k)$, the phase shift $\varphi(k)$ and the mean free path of the photoelectron $\lambda(k)$ were calculated from *FEFF9* (Ankudinov *et al.*, 1998). The reduction factor S_0^2 was set as 1. The range of k was 2–14 Å^{-1}. To ensure the stability of this method, random noise was added to $\chi(k)$. The random noise was produced by $10^{-4} \times \mathrm{randn}(k)$, where randn(...) is a function to generate normally distributed random numbers. Kernel K and data were both weighted by k^3.

In Fig. 1(*a*), the solid line is the theoretical $g(r)$. Three peaks have merged into a single peak and become indistinguishable. Fig. 1(*b*) shows the theoretical EXAFS data $\chi(k)$ with added noise and the fitting curve. The dashed line is a Hanning window for the FT with a window parameter of 20. Fig. 1(*c*) shows the reconstructed ADF and the phase- and amplitude-corrected FT spectrum (van Zon *et al.*, 1984) of the simulated data. While the three peaks are indistinguishable using the FT method, they are successfully resolved by the ADF method. In the ADF method, the peak position and peak area are the bond length and coordination number, respectively. Calculated parameters are $n_1 = 2.0$, $n_2 = 2.1$, $n_3 = 2.0$, $r_1 = 1.915$ Å, $r_2 = 2.007$ Å, $r_3 = 2.082$ Å, $\sigma^2 = 0.0049$ Å^2, which are very close to the true values. The maximum bias of the bond length is only 0.008 Å. Considering that the noise added is higher than usually recorded in real experimental data and the results are close to the true values, our method should be regarded as stable and reliable.

3.2. Testing using the $LaFe_{1-x}Cr_xO_3$ system

For further testing of our method, perovskite materials were chosen. Perovskite materials exhibit many interesting properties from both theoretical and application points of view. CMR, ferroelectricity, superconductivity, charge ordering, spin-dependent transport and high thermopower are commonly observed features in this kind of material. As one of the most widely used perovskite structures, the perovskite oxides ABO_3, containing a rare-earth metal on the A sites with 12-fold oxygen coordination and a transition metal on the B sites with six-fold oxygen coordination, exhibit a rich variety of unusual and interesting electronic, magnetic and structural properties (Andreasson *et al.*, 2007). In this contribution, we chose the $LaFe_{1-x}Cr_xO_3$ system which is well known because of its 'strange' magnetic behaviour (Ueda *et al.*, 1998). For a long time, ferromagnetism (FM) was expected to be found in $LaFe_{1-x}Cr_xO_3$ but it was not observed until a $LaFeO_3$–$LaCrO_3$ superlattice was obtained in 1998 (Ueda *et al.*, 1998). It is generally believed that FM is absent in such materials due to

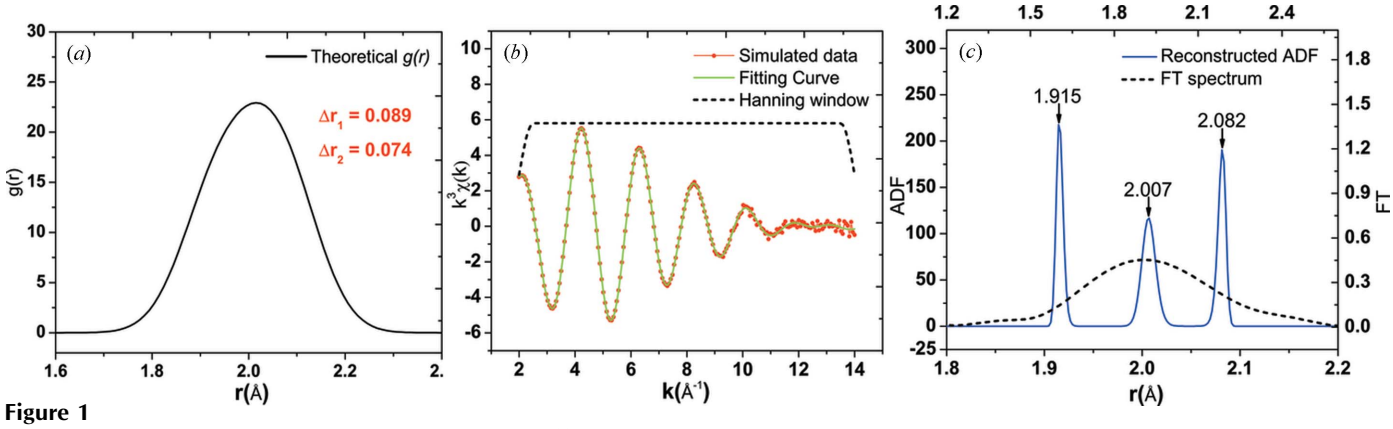

Figure 1
Validation of our method using numerical simulations. (*a*) $g(r)$ is the theoretical curve built using three Gaussian peaks with $n_1 = n_2 = n_3 = 2$, $r_1 = 1.923$, $r_2 = 2.012$, $r_3 = 2.086$, $\sigma^2 = 0.005$. Δr_1 is the bond length difference between r_1 and r_2. Δr_2 is the bond length difference between r_2 and r_3. To resolve these three peaks, a spatial resolution better than the smallest one, Δr_2, is needed. These three peaks merged into a single peak which is indistinguishable using existing EXAFS data analysis methods. (*b*) Simulated data are the EXAFS data $\chi(k)$ calculated using equation (1) with added noise. Data are k^3-weighted. The fitting curve is the curve fitted by our algorithm. A Hanning window for the FT is shown as a dashed line and the window parameter is 20. (*c*) The dashed line shows the phase- and amplitude-corrected FT spectrum (van Zon *et al.*, 1984) of the simulated data. The three peaks are indistinguishable using this method. The solid line shows the atom distribution function (ADF) calculated from our method. The peaks are clearly resolved. The peak position and the area are the bond length and coordination number, respectively. Calculated parameters are $n_1 = 2.0$, $n_2 = 2.1$, $n_3 = 2.0$, $r_1 = 1.915$ Å, $r_2 = 2.007$ Å, $r_3 = 2.082$ Å, $\sigma^2 = 0.0049$ Å^2, which are very close to the true values.

the fact that FM coupling of Fe–O–Cr has not been achieved when synthesizing such materials by sintering methods. The materials phase separates into Fe oxide and Cr oxide phases (Ueda *et al.*, 1998; Wold & Croft, 1959). As a result, a ferromagnetic-ordered phase has not been obtained. In this work, powder samples of $LaFe_{1-x}Cr_xO_3$ (x = 0, 1/3, 2/3) were synthesized using a standard solid-state reaction method (Belayachi *et al.*, 1996; Louca *et al.*, 1999). X-ray diffraction spectra indicated that all samples crystallize in the perovskite structure with orthorhombic deformation, having a space group *Pbnm* (Wang *et al.*, 2007).

The procedure to resolve the EXAFS data using our method is as follows.

(1) Conventional EXAFS data treatment, including background correction, E–k space conversion, μ_0-fit, Fourier transform and inverse Fourier transform (IFT). XAFS data analysis software, such as *WinXAS*, *IFEFFIT etc.*, can be used to perform this.

(2) Reconstruct the ADF using filtered EXAFS data.

In this example, *WinXAS* was used to carry out the conventional data analysis. For the IFT, the data range was set at 1.15–2.10 Å to filter the EXAFS data of the first main peak which mainly consists of Fe–O octahedral coordinations. Fig. 2(*a*) shows the FT data of $LaFe_{1-x}Cr_xO_3$. Fig. 2(*b*) shows the filtered EXAFS data of Fe–O peaks. All data were weighted by k^3. Fig. 2(*d*) shows the reconstructed ADF. The calculated bond lengths of $LaFeO_3$ were 1.919, 2.007 and 2.087 Å. The maximum error was 0.005 Å with the X-ray diffraction data of Sangaletti *et al.* (2001). Further detailed structure information is shown in Table 1. Based on the reconstructed ADF, a lattice distortion model of octahedral FeO_6 with Cr doping was obtained and is shown in Fig. 2(*e*).

From Fig. 2(*d*) we can see that the Fe–O octahedral structure changes as a function of Cr doping. This is a clear evidence that Fe atoms were replaced by Cr atoms. Furthermore, the three FT spectra in Fig. 2(*a*) look similar, indicating that the three samples have similar structures. Combining the structural analysis of Fe–O and the FT spectra, our results indicate that ferromagnetic coupling of Fe–O–Cr is present and phase separation is not the real reason for the absence of FM in the $LaFe_{1-x}Cr_xO_3$ sample. In another paper (Belayachi *et al.*, 1998), the authors found an unusual magnetic behaviour in $LaFe_{1-x}Cr_xO_3$ when $x > 0.5$. In Fig. 2(*d*), we can see that the Fe–O octahedral structure changes significantly when x = 2/3, indicating that the unusual magnetic behaviour may be related to the Fe–O octahedral distortion.

In this section, our method was examined by using theoretical data based on $LaFeO_3$ and experimental data of $LaFe_{1-x}Cr_xO_3$, requiring a spatial resolution better than 0.074 Å. For theoretical data and $LaFeO_3$ standard data, the three subshells were resolved clearly and the maximum bond length errors were only 0.008 Å and 0.005 Å, respectively. This clearly indicates that our method has good spatial resolution and the calculated results are reliable.

4. Discussion and summary

EXAFS is an advanced technique which is sensitive to local structure around the absorbing atoms. In this paper, we focus on the nearest subshells only and achieve a spatial resolution higher than 0.1 Å. To obtain sub-10 pm resolution, our method requires the same atom species of the subshells, otherwise the kernel function cannot be regarded as the same for different subshells and the algorithm cannot be applied. Therefore our method is suitable for studying MO_6 octahedral distortion. Regarding the algorithm to resolve equations (6)–(8), the one we have introduced in this paper is based on the gradient descent algorithm. The testing of our method to analyze numerical simulation data shows that a resolution better than 6 pm cannot be obtained using 12 Å^{-1} data (the

Table 1
Fitting parameters of experimental data of $LaFe_{1-x}Cr_xO_3$ (x = 0, 1/3, 2/3).

n_1, n_2, n_3 and r_1, r_2, r_3 are the coordination numbers and bond lengths of the three subshells, respectively. σ^2 is the DWF.

	n_1	r_1 (Å)	n_2	r_2 (Å)	n_3	r_3 (Å)	$\sigma^2 \times 10^3$ (Å^2)
$LaFeO_3$‡	2	1.923	2	2.012	2	2.086	
x = 0	1.5 ± 0.1	1.919 ± 0.001	2.6 ± 0.2	2.007 ± 0.002	1.9 ± 0.2	2.087 ± 0.001	0.5 ± 0.1
x = 1/3	1.0 ± 0.1	1.898 ± 0.0005	3.5 ± 0.3	1.999 ± 0.002	1.5 ± 0.1	2.094 ± 0.001	0.5 ± 0.1
x = 2/3	0.5 ± 0.07	1.891 ± 0.001	3.2 ± 0.3	1.973 ± 0.002	2.3 ± 0.2	2.069 ± 0.002	0.5 ± 0.1

‡ Structural information calculated from Sangaletti *et al.* (2001).

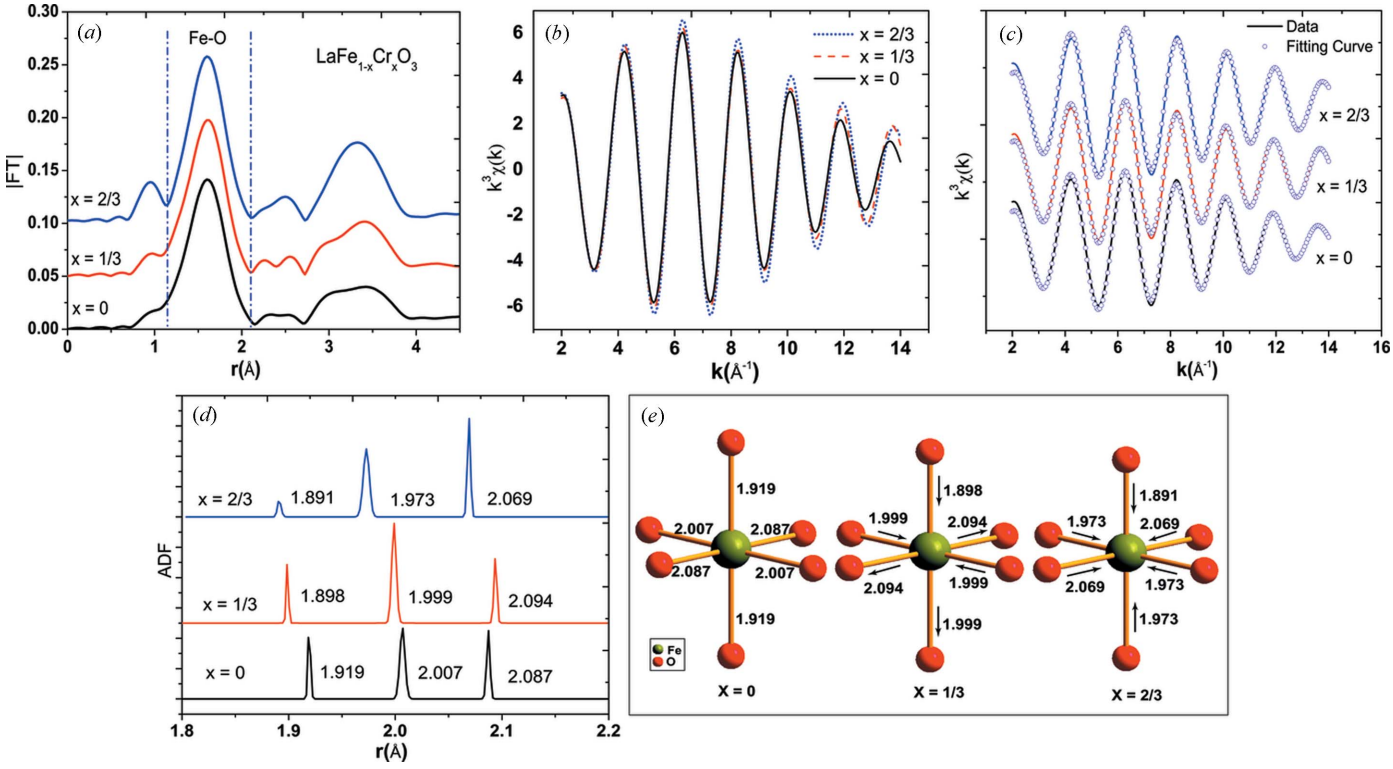

Figure 2
Data analysis of the $LaFe_{1-x}Cr_xO_3$ system with x = 0, 1/3, 2/3. (*a*) Fourier transform of $LaFe_{1-x}Cr_xO_3$ EXAFS spectra. (*b*) EXAFS functions of the first coordination shell obtained by inverse FT over a filtered range between 1.15 and 2.10 Å. All data are k^3-weighted. (*c*) EXAFS data along with the fitting curves obtained using our algorithm. (*d*) Reconstructed ADF. Peak positions are indicated. Structural parameters are summarized in Table 1. (*e*) FeO_6 octahedral distortion model obtained based on the reconstructed ADF. Bond lengths of Fe–O and distortion direction of each O atom are shown in the figure.

theoretical resolution limit is about 4.2 pm). For the next step, we will apply the regularization method to resolve equations (6)–(8) in an attempt to achieve a closer approximation to the resolution limit.

In summary, we have developed a new EXAFS data analysis method which is based on a non-parametrical algorithm allowing one to obtain structural information directly from EXAFS data without assuming the number of fitting parameters. Theoretically, the resolution limit of our method is $\Delta r \geq (1/2)\Delta k$, which is three times better than the existing methods. Hence, we are able to perform structural analysis at the 4.2 pm scale or smaller using EXAFS as we can collect data over a 12 Å^{-1} range or higher easily using advanced synchrotron radiation facilities. Furthermore, our method can be easily extended to study lattice distortion caused by vacancy, temperature, pressure and size effects or other systems which require high spatial resolution. Our method is expected to help scientists to understand the relationship between material properties and structures at the limit potential of EXAFS.

EXAFS data were collected at beamline 1W1B of the Beijing Synchrotron Radiation Facility and the XAFCA facility at Singapore Synchrotron Light Source. The authors are very grateful to Professor Yuhui Dong, Professor Jing Zhang, Professor Gopinathan Sankar, Dr Tao Liu and Dr Ping Yang for the stimulating discussions. This research was financially supported by the Strategic Priority Research

Program of the Chinese Academy of Science (Grant No. XDB10020100) and the Agency for Science, Technology and Research (A*Star) of Singapore.

References

Andreasson, J., Holmlund, J., Knee, C. S., Käll, M., Börjesson, L., Naler, S., Bäckström, J., Rübhausen, M., Azad, A. K. & Eriksson, S.-G. (2007). *Phys. Rev. B*, **75**, 104302.

Ankudinov, A. L., Ravel, B., Rehr, J. J. & Conradson, S. D. (1998). *Phys. Rev. B*, **58**, 7565–7576.

Babanov, Yu. A., Vasin, V. V., Ageev, A. L. & Ershov, N. V. (1981). *Phys. Status Solidi B*, **105**, 747–754.

Belayachi, A., Loudghuu, E., Elyamani, M., Nogues, M., Dormann, J. L. & Taibi, M. (1996). *Eur. J. Solid State Inorg. Chem.* **33**, 1039–1049.

Belayachi, A., Loudghiri, E., Elyamani, M., Nogues, M., Dormann, J. L. & Taibi, M. (1998). *Ann. Chim. Sci. Mater.* **23**, 297–300.

Booth, C. H., Bridges, F., Kwei, G. H., Lawrence, J. M., Cornelius, A. L. & Neumeier, J. J. (1998). *Phys. Rev. Lett.* **80**, 853–856.

Chu, W., Cheng, J., Chu, S., Hu, T., Marcelli, A., Chen, X. & Wu, Z. (2013). *Sci. Rep.* **3**, 1750.

Cruz, C. de la, Hu, W. Z., Li, S., Huang, Q., Lynn, J. W., Green, M. A., Chen, G. F., Wang, N. L., Mook, H. A., Si, Q. & Dai, P. (2010). *Phys. Rev. Lett.* **104**, 017204.

Dalba, G., Fornasini, P., Grisenti, R. & Purans, J. (1999). *Phys. Rev. Lett.* **82**, 4240–4243.

Fábián, M., Sváb, E., Mészáros, Gy., Révay, Zs., Proffen, Th. & Veress, E. (2007). *J. Non-Cryst. Solids*, **353**, 2084–2089.

Funke, H., Chukalina, M. & Scheinost, A. C. (2007). *J. Synchrotron Rad.* **14**, 426–432.

Gupta, K., Mahadevan, P., Mavropoulos, P. & Lezaić, M. (2013). *Phys. Rev. Lett.* **111**, 077601.

Haas, O., Struis, R. P. W. J. & McBreen, J. M. (2004). *J. Solid State Chem.* **177**, 1000–1010.

Lee, P. A., Citrin, P. H., Eisenberger, P. & Kincaid, B. M. (1981). *Rev. Mod. Phys.* **53**, 769–806.

Louca, D., Sarrao, J. L., Thompson, J. D., Röder, H. & Kwei, G. H. (1999). *Phys. Rev. B*, **60**, 10378.

Pandey, S. K., Khalid, S., Lalla, N. P. & Pimpale, A. V. (2006). *J. Phys. Condens. Matter*, **18**, 10617–10630.

Penfold, T. J., Tavernelli, I., Milne, C. J., Reinhard, M., El Nahhas, A., Abela, R., Rothlisberger, U. & Chergui, M. (2013). *J. Chem. Phys.* **138**, 014104.

Rossberg, A. & Funke, H. (2010). *J. Synchrotron Rad.* **17**, 280–288.

Saha, S. R., Butch, N. P., Kirshenbaum, K. & Paglione, J. (2009). *Phys. Rev. Lett.* **103**, 037005.

Sangaletti, L., Depero, L. E., Allieri, B., Nunziante, P. & Traversa, E. (2001). *J. Eur. Ceram. Soc.* **21**, 719–726.

Sayers, D. E., Stern, E. A. & Lytle, F. W. (1971). *Phys. Rev. Lett.* **27**, 1204–1207.

Sen, C., Alvarez, G. & Dagotto, E. (2010). *Phys. Rev. Lett.* **105**, 097203.

Stern, E. (2001). *J. Synchrotron Rad.* **8**, 49–54.

Sundaram, N., Jiang, Y., Anderson, I. E., Belanger, D. P., Booth, C. H., Bridges, F., Mitchell, J. F., Proffen, Th. & Zheng, H. (2009). *Phys. Rev. Lett.* **102**, 026401.

Teo, B. K. (1986). *EXAFS: Basic Principles and Data Analysis.* New York: Springer-Verlag.

Tikhonov, A. N. & Arsenin, V. Ya. (1981). *Solution of Ill-Posed Problems.* New York: John Wiley and Sons.

Toby, B. H. & Egami, T. (1992). *Acta Cryst.* A**48**, 336–346.

Ueda, K., Tabata, H. & Kawai, T. (1998). *Science*, **280**, 1064–1066.

Wang, J.-O., Du, Y., Ibrahim, K., Hong, C., Xie, Y. & Hu, T. (2007). *Chin. Phys. C*, **31**, 101–103.

Wang, Y. F. (2007). *Computational Methods for Inverse Problems and their Applications.* Beijing: Higher Education Press.

Wold, A. & Croft, W. (1959). *J. Phys. Chem.* **63**, 447–448.

Yang, D. S. & Bunker, G. (1996). *Phys. Rev. B*, **54**, 3169–3172.

Zon, J. B. A. D. van, Koningsberger, D. C., Prins, R. & Sayers, D. E. (1984). *Springer Proc. Phys.* **2**, 89–91.